

SN 2014C: VLBI Images of a Supernova Interacting with a Circumstellar Shell

Michael F. Bietenholz^{1,2}, Atish Kamble³, Raffaella Margutti⁴, Danny Milisavljevic³,
Alicia Soderberg³

¹*Hartebeesthoek Radio Observatory, PO Box 443, Krugersdorp, 1740, South Africa*

²*Department of Physics and Astronomy, York University, Toronto, M3J 1P3, Ontario, Canada*

³*Harvard-Smithsonian Center for Astrophysics, 60 Garden Street, Cambridge, MA 02138, USA*

⁴*Center for Interdisciplinary Exploration and Research in Astrophysics (CIERA) and Department of Physics and Astronomy, Northwestern University, Evanston, IL 60208, USA*

Accepted to *MNRAS*; 14 July 2021

ABSTRACT

We report on VLBI measurements of supernova 2014C at several epochs between $t = 384$ and 1057 days after the explosion. SN 2014C was an unusual supernova that initially had Type Ib optical spectrum, but after $t = 130$ d it developed a Type IIn spectrum with prominent H α lines, suggesting the onset of strong circumstellar interaction. Our first VLBI observation was at $t = 384$ d, and we find that the outer radius of SN 2014C was $(6.40 \pm 0.26) \times 10^{16}$ cm (for a distance of 15.1 Mpc), implying an average expansion velocity of 19300 ± 790 km s⁻¹ up to that time. At our last epoch, SN 2014C was moderately resolved and shows an approximately circular outline but with an enhancement of the brightness on the W side. The outer radius of the radio emission at $t = 1057$ d is $(14.9 \pm 0.6) \times 10^{16}$ cm. We find that the expansion between $t = 384$ and 1057 d is well described by a constant velocity expansion with $v = 13600 \pm 650$ km s⁻¹. SN 2014C had clearly been substantially decelerated by $t = 384$ d. Our measurements are compatible with a scenario where the expanding shock impacted upon a shell of dense circumstellar material during the first year, as suggested by the observations at other wavelengths, but had progressed through the dense shell by the time of the VLBI observations.

Key words: Supernovae: individual (SN 2014C) — radio continuum: general

1 INTRODUCTION

A complex picture has been emerging of the ends of the lives of massive stars, and how they shed matter in stellar winds before undergoing a core-collapse supernova (SN) explosion. It is often assumed that the stellar winds are relatively steady, leading to a circumstellar medium (CSM) with density, $\rho \propto r^{-2}$ (e.g. Weaver et al. 1977; Chevalier 1982b; Dwarkadas 2005; Chevalier & Irwin 2011). However, recently evidence has been mounting that many massive stars experience highly variable stellar winds and eruptive mass-loss in the period before the explosion (see Smith 2014, for a review). The stellar winds are driven from the surface of the star, whereas the processes leading up to the core collapse occur deep in the interior, so it is unclear what drives mass-loss events shortly before the SN explosions.

In the case of Type Ib/c SNe, the so-called “stripped-envelope” SNe, which arise from stars that have lost much

of their H envelopes prior to the explosion, evidence for non-steady mass loss shortly prior to the explosion has been seen in several SNe. In particular, modulated radio lightcurves have been seen in several Type I b/c SNe (Soderberg et al. 2006; Wellons et al. 2012; Milisavljevic et al. 2013), which suggest modulations in the CSM density as a function of radius and therefore temporal variation of the mass-loss in the period preceding the SN explosion.

SN 2014C is a particularly interesting case. It was discovered on 2014 January 5 (Kim et al. 2014) in the nearby early-type spiral galaxy NGC 7331 by the Lick Observatory Supernova Search. We adopt the updated Cepheid distance of $D = 15.1 \pm 0.7$ Mpc from Saha et al. (2006). We also adopt an explosion date, $t = 0$, of 2013 December 30.0 (UT) = MJD 56656.0, as determined by Margutti et al. (2017) from bolometric lightcurve modelling.

At the time of its discovery, SN 2014C’s spectrum was

that of an ordinary, H-stripped Type Ib supernova (Kim et al. 2014; Tartaglia et al. 2014), but over the next year it evolved into a Type IIn spectrum showing prominent H α -lines indicating strong CSM interaction (Milisavljevic et al. 2015; Margutti et al. 2017). It also, unusually, kept brightening in X-rays till $t \sim 1$ yr (Margutti et al. 2017), and H α emission was still detected as late as $t \simeq 892$ d (Vinko et al. 2017). In the mid-infrared, it had an almost constant brightness till $t \sim 800$ d, with even a possible slight re-brightening near $t \sim 250$ d (Tinyanont et al. 2016).

It was detected early on in radio, both at 7 GHz by the Very Large Array (Kamblé et al. 2014), and at 85 GHz by Combined Array for Research in Millimeter Astronomy (Zauderer et al. 2014). A 16-GHz radio lightcurve from the Arcminute Microkelvin Imager was presented by Anderson et al. (2017), who found a very unusual two-peaked lightcurve, with the first peak at $t \simeq 80$ d, and a second at $t \simeq 400$ d. A paper on our multi-frequency flux-density monitoring of SN 2014C with the Jansky Very Large Array is in preparation (Kamblé et al.).

Milisavljevic et al. (2015) and Margutti et al. (2017) suggest a scenario where SN 2014C's progenitor exploded inside a relatively low-density cavity, but within a year, the expanding shock encountered a massive H-rich shell (probably $\sim 1 M_{\odot}$) at radius, $r_{16} \sim 6$, where r_{16} is a dimensionless radius, and $r_{16} = r/(10^{16} \text{ cm})$. Such a shell is not expected from the standard metallicity-dependent line-driven mass-loss scenario (Kudritzki & Puls 2000; Nugis & Lamers 2000), and requires a different, highly time-dependent mass-loss mechanism that is active during the last centuries before the explosion.

A key ingredient to understanding SN 2014C is knowing basic parameters, in particular the (time-dependent) radius of the expanding ejecta and the corresponding expansion speed. Very contradictory values have been proposed: Anderson et al. (2017) suggest values of r_{16} of 0.332 ± 0.007 , based on modelling the lightcurve bumps on the assumption that the dominant absorption mechanism is synchrotron self-absorption (SSA), although they do warn that this assumption may not be appropriate for SN 2014C. The size reported by Anderson et al. would imply relatively low average expansion velocities of $\lesssim 5000 \text{ km s}^{-1}$ for $t = 80$ d, whereas typically Type Ib SNe have velocities several times higher (e.g. Chevalier 2007; Bietenholz 2014b). As mentioned, there is considerable evidence of SN 2014C's shock impacting on a dense shell of circumstellar material (CSM) between $t = 30 \sim 130$ d after the explosion, which would likely entail high shock velocities in the period before the impact. For example, an average speed¹ of 49000 km s^{-1} , which is an order of magnitude higher than the value implied by Anderson et al., ensues from Margutti et al. (2017)'s particular values for the time of the shock's impact on the shell, 130 d, and its radius, $r_{16} \sim 5.5$.

VLBI observations are the only way to resolve the forward shock and to therefore obtain direct observational con-

straints on its size, and thus also on the shock velocity. We therefore undertook VLBI observations of SN 2014C with the goals of determining the radius at various times.

The VLBI observations also hold the promise of revealing the morphology of the radio emission. There are only a handful of SNe where the radio emission can be resolved (see Bartel & Bietenholz 2016; Bietenholz 2014a, for recent reviews), so given SN 2014C's close distance and bright radio emission, it held the promise of adding to our catalogue of SNe with resolved emission.

2 OBSERVATIONS AND DATA REDUCTION

We obtained four VLBI observing sessions on SN 2014C with the National Radio Astronomy Observatory (NRAO)² High Sensitivity Array (HSA) between 2015 January and 2016 April. We give the particulars of the observing runs in Table 1.

The HSA includes the Robert C. Byrd telescope at Green Bank, GB (~ 105 m diameter). At the time of our observations, GB was affected by a bug, that caused GB phases to reset at the start of each scan, and therefore rendered phase-referencing impossible for GB data. The GB data could be recovered by self-calibrating in phase on a per-scan basis if the signal-to-noise was high enough. In the cases where this was possible we did so, and our images and model-fitting results are based on this self-calibrated data. Where such self-calibration was not possible we excluded the GB data. All our astrometric results are based on un-self-calibrated data excluding GB.

We observed at both 8.4 and 22.1 GHz, recording both senses of circular polarization over a bandwidth of 256 MHz. As usual, a hydrogen maser was used as a time and frequency standard at each telescope, and we recorded with the RDBE/Mark5C wide-band system at a sample-rate of 2 Gbps, and correlated the data with NRAO's VLBA DiFX correlator. All the observing runs were 8 h in length, with the time was divided approximately equally between observations at 22 and 8.4 GHz for the two runs in 2015, while in 2016 we observed only at 8.4 GHz.

We phase-referenced our observations to the sources VCS3 J2235+3418, 0.24° away from SN 2014C, and VCS1 J2248+3718, 2.90° away. We will refer to the two just as J2235+3418 and J2248+3718, respectively. We used J2235+3418 as a primary reference source at 8.4 GHz, as it is closer on the sky. However, at 22 GHz it is too weak for reliable phase-referencing, so we used the stronger but somewhat more distant J2248+3718. We included some scans of J2235+3418 at 22 GHz and of J2248+3718 at 8.4 GHz. This served two purposes: firstly it allows us to align the images at the two frequencies accurately, and secondly allows us to check for any possible proper motion of the reference sources.

The data reduction was carried out with NRAO's Astronomical Image Processing System (AIPS). The initial flux density calibration was done through measurements of the system temperature at each telescope, and improved through self-calibration of the phase-reference sources.

¹ Note that Margutti et al. (2017) give a value of 44000 km s^{-1} for the instantaneous velocity of the forward shock when it impacts on the shell; our value, which is merely the radius divided by the time, is the *average* value between the time of the explosion and the time of impact, and is slightly higher than the instantaneous value because the shock is decelerating.

² The National Radio Astronomy Observatory, NRAO, is a facility of the National Science Foundation operated under cooperative agreement by Associated Universities, Inc.

Table 1. VLBI Observations of SN2014C

Date	Proposal code ^a	Telescopes ^b	MJD ^c	Freq. (GHz)	Total flux density ^e (mJy)	Peak ^d Brightness (mJy beam ⁻¹)	Image rms (μ Jy beam ⁻¹)	Convolving beam FWHM (mas \times mas, $^\circ$)
2015 Jan 17	14B-500	VLBA, GB	57039.8	22.1	17.8	9.0	103	$0.68 \times 0.33, 12^\circ$
2015 Jan 17	14B-500	VLBA, GB	57039.8	8.4	25.2	21.7	80	$1.55 \times 0.80, -3^\circ$
2015 Oct 05	15B-312	VLBA, GB ^f	57301.2	22.1	no image made due to GB phasing problems			
2015 Oct 05	15B-312	VLBA, GB ^{f,g}	57301.2	8.4	26.4	20.0	80	$1.55 \times 0.80, -3^\circ$
2016 Apr 30	15B-312	VLBA, GB, Y, EB	57508.5	8.4	23.0	15.6	27	$1.55 \times 0.80, -3^\circ$
2016 Nov 20	15B-312	VLBA, GB, Y, EB	57713.0	8.4	22.8	8.8	21	$1.32 \times 0.44, -12^\circ$

^a NRAO observing code

^b VLBA = NRAO Very Long Baseline Array, 10×25 m diameter; GB = Robert C. Byrd telescope at Green Bank, ~ 105 m diameter; Y = the Jansky Very Large Array in phased-array mode, equivalent diameter 94 m; EB = the Effelsberg antenna, 100 m diameter.

^c Modified Julian Date of midpoint of observation

^d Total (CLEANed) flux density in image

^e The peak brightness in the image

^f EB and Y were scheduled, but the observations failed

^g The image was super-resolved by $\sim 6\%$ to match the resolution of other images

3 VLBI IMAGES

We show a sequence of the first three 8.4-GHz VLBI images of SN 2014C from 2015 January 17 to 2016 April 30 ($t = 384 - 852$ d) in Figure 1, and the 8.4-GHz image from 2016 November 6 ($t = 1057$ d) in Figure 2. The total flux densities, peak brightnesses, and background rms brightness values are given in Table 1. The images were deconvolved using the CLEAN algorithm, with AIPS robustness parameter set to -4 which gives a weighting close to uniform. To increase the reliability of the images we used the square root of the data weights in the imaging, which results in more robust images less dominated by a few very sensitive baselines in the HSA.

For our last image (2016 November 6, Figure 2), the total CLEANed flux density was 22.8 mJy, the peak brightness was $8.81 \text{ mJy beam}^{-1}$, and the rms of the background brightness was $21 \mu\text{Jy beam}^{-1}$. The FWHM resolution or CLEAN beam was somewhat elongated due to the low declination of the source, and was of 1.32×0.44 mas at p.a. -15° . At this epoch, SN 2014C is moderately resolved in an approximately E-W direction with the E-W extent of the source (estimated by the 50% contour) being ~ 3 times the FWHM resolution. In the perpendicular direction, the source diameter is comparable to the resolution.

Although the lower brightness contours of SN 2014C in Figure 2 are relatively elongated, this is merely due to the convolution with the elongated CLEAN beam. The 50% contour of the image, which would correspond approximately to the perimeter of a hard-edged source, is more circular, suggesting that the true source shape is likely not greatly elongated. There is a distinct brightness enhancement on the W side of the source. Since the dynamic range of this image is quite high, this enhancement is almost certainly real as it is much larger than either the off-source noise or any expected deconvolution artefacts.

4 SIZE, EXPANSION SPEED AND PROPER MOTION

Although SN 2014C is moderately resolved in our last VLBI image, it is less so in our earlier images, and we turn to fitting geometrical models in the Fourier transform or u - v plane to most accurately determine the size evolution. Bietenholz et al. (2010) showed that in the case of SN 1993J, the results obtained through u - v plane model fitting are superior to those obtained in the image plane. We again used the square root of the data weights in the fitting, which makes the results more robust at the expense of some statistical efficiency. We used the AIPS task OMFIT to fit the models.

The expected structure of the radio emission of a SN is that of a spherical shell, with the radio emission arising between the forward shock which is driven into the CSM and a reverse shock that is driven back into the freely-expanding ejecta. Indeed, the few SNe that have been reasonably resolved mostly show a morphology approximately consistent with a projected spherical shell, albeit usually with some localized brightness enhancements along the ridge of the projected shell (see, e.g. Bietenholz 2014a). Our last image of SN 2014C (Fig. 2) indeed also shows a structure that can also be interpreted within this context, although it does show a distinct departure from circular symmetry in the presence of a brightness enhancement on the W side.

If the supernova is optically thick, then the expected morphology is closer to a uniform disk. This was the case for our 2015 Jan. epoch at 8.4 GHz, as can be seen from the SED in Margutti et al. (2017), which shows that the turnover frequency was around 20 GHz at that time. We did fit both a disk and a spherical shell model to the 2015 Jan. data and found that indeed the disk model fitted better for the 8.4-GHz data, at which frequency the SN was still optically thick, while the shell model fitted better at 22 GHz, where the SN was optically thin. However, the fractional difference in χ^2 between the two models was very small ($< 10^{-3}$) so we do not consider the difference significant. The fitted outer radii are expected to be very similar for the two models, and indeed our fitted outer radius values agreed to within half the uncertainties. For the sake of consistency, we were therefore

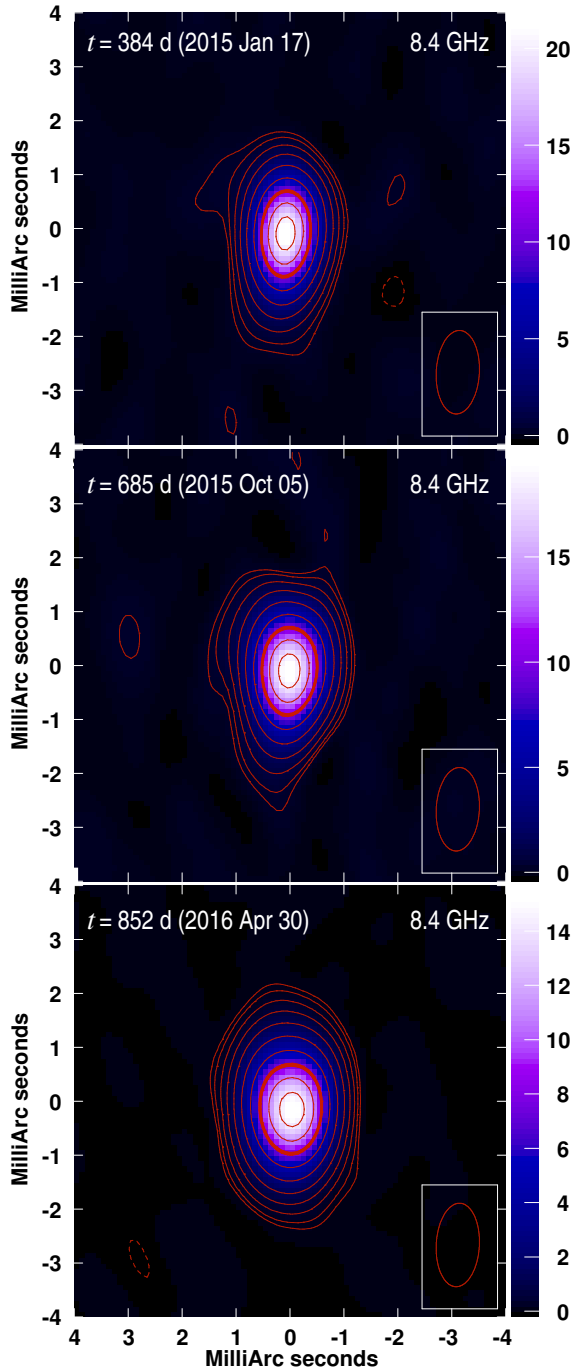


Figure 1. The 8.4-GHz VLBI images from 2015 January 17, 2015 October 05 and 2016 April 30, all rendered at a common FWHM resolution of 1.55×0.8 mas at p.a. -3° , indicated at lower left in each pane. Both the contours and the colorscale show the image brightness, the latter labelled in mJy beam^{-1} . The total CLEANed flux densities, peak brightnesses, rms backgrounds and CLEAN beams are given in Table 1. For 2015 January 17 and 2015 October 5, the contours are at $-1, 1, 2, 4, 8, 16, 30, 50$ (emphasized), 70 and 90%, of the peak brightness. The 2015 October 5 image was super-resolved by $\sim 6\%$ to match the resolution of the others. For 2016 April 30, the contours are as for the previous two except the lowest contours are at $-0.6, 0.6$ and 1% .

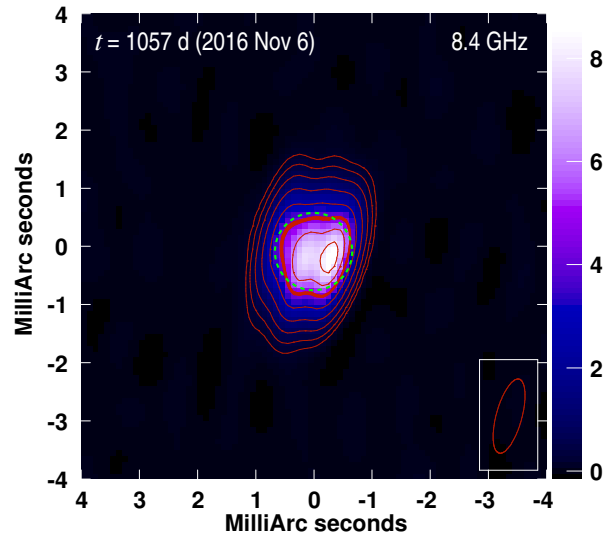


Figure 2. The 8.4-GHz VLBI Image from 2016 November 6 or $t = 1057$ d. The total CLEANed flux density was 22.8 mJy, and the rms of the background brightness was $21 \mu\text{Jy beam}^{-1}$. Both the contours and the colour show the image brightness, with the colorscale being labelled in mJy beam^{-1} . The contours, in red, are at $-1, 1, 2, 4, 8, 16, 30, 50$ (emphasized), 70 and 90% of the peak brightness, which was $8.81 \text{ mJy beam}^{-1}$. The FWHM resolution of 1.32×0.44 mas at p.a. -15° is indicated at lower left. The dashed (green) circle shows the outer radius of a fitted spherical shell model (see text, §4).

use only the values from the spherical shell model below, since those should be more appropriate for most epochs and frequencies, and as we have shown the differences are small even if the SN is still optically thick.

The data do not reliably determine the thickness of the spherical shell even at our last epoch when the SN is most resolved, so we assume a thickness of 20% of the outer radius, which has been shown to be appropriate in the case of SN 1993J (Bietenholz et al. 2003; Bartel et al. 2007), and is near the value expected on theoretical grounds in the case of a simple CSM structure (Chevalier 1982a; Jun & Norman 1996). Our fitted outer radius is only weakly dependent on the assumed shell thickness, and reasonable deviations from the assumed value of 20% will not change our outer radii by more than our stated uncertainties.

We use the outer radius of this fitted spherical shell model to estimate the outer radius of SN 2014C. The purely statistical uncertainties on the fitted sizes were small in all cases ($\lesssim 0.010$ mas). Given the approximate nature of the shell model and the fact that, because of the antenna-dependent gain calibration, the calibrated visibility measurements are not statistically independent, systematic contributions will dominate the uncertainty in the fitted sizes. We estimated two different contributions to the systematic uncertainties, which we add in quadrature to the statistical one for our total uncertainties.

The first contribution was estimated using jackknife resampling (McIntosh 2016). Specifically, we dropped the data from each of the antennas in the VLBI array in turn and calculated N_{antenna} new estimates of the fitted size, and the scatter over these N_{antenna} values allows one to estimate the

uncertainty of the original value which included all antennas. Since the uncertainty should scale with the resolution, we compared the results to the FWHM resolution, for which we take the geometric mean of the major and minor axes of the fitted restoring beam. We carried out this procedure for four epochs, 2015 Jan. 17, 22 GHz; 2015 Oct. 05, 8.4 GHz, 2016 Apr. 30, 8.4 GHz and 2016 Nov. 20, 8.4 GHz, and obtained estimates of the uncertainty of 2.1, 1.2, and 1.2 and 4.2% of FWHM resolution for the three epochs respectively. Based on this test, we took a rounded 2% of the geometric mean of the major and minor axes of the restoring beam as the uncertainty for all epochs.

The second contribution is an estimate of the effect of any gain mis-calibration on the fitted sizes. For marginally resolved sources, such as SN 2014C, the fitted size is correlated with the antenna gains, which are not exactly known. We estimated this contribution to the uncertainty in a Monte-Carlo fashion by repeatedly randomly varying the individual antenna gains by 10% (rms), and then re-fitting the spherical shell models. This estimate should be conservative as it is unlikely that our antenna gains would be wrong by as much as 10%.

We give the fitted outer radii and the total uncertainties in Table 2, and plot them in Figure 3. For our last epoch ($t = 1057$ d), we also plot a circle showing the outer radius of the fitted model in Figure 2 to show the relation between the fitted model and the VLBI image.

Given the brightness enhancement to the W seen in the $t = 1057$ d image, the circularly symmetric spherical shell model is clearly only an approximate description of SN 2014C. However, barring any gross changes in the morphology as it expands, our fitted radii should give a reliable picture of the expansion of the SN.

For the first two epochs, we had observations at both 22.1 and 8.4 GHz. In both cases we found that the radii measured at 8.4 GHz were $\sim 20\%$ larger than the corresponding 22-GHz ones, however, the difference is only $\sim 1\sigma$ in each case. Absorption is strongly frequency dependent, and so might cause a variation with frequency of the apparent size. If SN 2014C were optically thick still at 8.4 GHz at these epochs ($t = 383, 645$ d), we would expect real brightness distribution to be approximately disk-like. If this case, our fit using a spherical shell model would slightly *underestimate* the true radius (for a discussion of this issue in the case of SN 1993J, see Bartel et al. 2002). However, the lower frequency should be more affected than the higher one, so in this case one would expect the fitted radii at the lower frequency to be too small, which is the opposite of what we find. We therefore consider it unlikely that absorption effects cause the differences of radius with frequency we find, which as mentioned, are of questionable significance.

Taking the weighted average of the radius measurements at 8.4 and 22 GHz of $(6.40 \pm 0.26) \times 10^{16}$ cm (for $D = 15.1$ Mpc), we find that the expansion speed between $t = 0$ d and 384 d was $(19300 \pm 790) \cdot (D/[15.1 \text{ Mpc}])$. Taking the differences between adjacent pairs of our VLBI epochs, we can calculate three further velocity values: $14500 \pm 3400 \text{ km s}^{-1}$, $12100 \pm 4700 \text{ km s}^{-1}$ and $14300 \pm 4200 \text{ km s}^{-1}$ at $t \simeq 514$ d, $\simeq 748$ d and $t \simeq 955$ d, respectively, all for $D = 15.1$ Mpc. At our last epoch at $t = 1057$ d, $r_{16} = (14.4 \pm 0.6) \cdot (D/(15.1 \text{ Mpc}))$.

Table 2. Radius Measurements

Date	MJD	Age (d)	Frequency (GHz)	Outer Radius ^a (mas)
2015 Jan 17	57039.8	384	22.1	0.280 ± 0.012
2015 Jan 17	57039.8	384	8.4	0.330 ± 0.045
2015 Oct 05	57301.2	645	22.1	0.359 ± 0.085
2015 Oct 05	57301.2	645	8.4	0.439 ± 0.034
2016 Apr 30	57508.5	852	8.4	0.524 ± 0.020
2016 Nov 20	57713.0	1057	8.4	0.636 ± 0.026

^a The angular outer radius of a spherical shell model, fitted directly to the visibility measurements in the Fourier-transform (u - v) plane by least-squares. The uncertainties consist of three parts, added in quadrature: the statistical uncertainty from the fit, 2% of the geometric mean of the major and minor axes (an estimated jackknife uncertainty obtained by dropping one antenna, see text), and the scatter in fitted radii obtained when randomly varying the antenna gains by 10%. In all cases, the statistical contribution is small compared to the other two.

4.1 Proper Motion

We take the fitted centre positions, obtained using only strictly phase-referenced data, as the best estimate of the centre position of SN 2014C at each epoch. Doing a least-squares fit over the positions of our four epoch results in proper motions of $-30, -12 \mu\text{as yr}^{-1}$ in RA and decl. respectively, with estimated uncertainties of $33 \mu\text{as yr}^{-1}$. For a distance of 15.1 Mpc, these proper motions translate to velocities of $-2100, -900 \text{ km s}^{-1}$ in RA and decl. respectively, with uncertainties of 2400 km s^{-1} . To within our uncertainties, then, the centre of SN 2014C is stationary.

4.2 Parametrization of the Expansion Curve

In order to parametrize the expansion curve using our measured radius values, we fitted our measured values of r_{16} with two different functions describing the evolution with time. We fitted these functions to our VLBI radius measurements using weighted least squares.

This first function, which we call the ‘‘powerlaw’’ function, is an uninterrupted powerlaw, $r = r_{1\text{yr}}(t/\text{yr})^m$, where r is the radius of the supernova at time, t , $r_{1\text{yr}}$ is the radius at $t = 1$ yr, and m is the powerlaw coefficient, often called the expansion parameter. Such a function is often used to describe the expansion of SNe, and many SNe do indeed show a shock radius expanding approximately in this fashion, with the best studied example being SN 1993J (e.g. Marcaide et al. 1997; Bartel et al. 2007; Bietenholz et al. 2010). Such a powerlaw evolution of the radius is in fact suggested on theoretical grounds. In a supernova, generally a dual shock structure is formed with a forward shock being driven into the CSM and a reverse shock back into the ejecta. It was shown that in the case that both the ejecta and CSM densities are powerlaws in radius, a self-similar evolution occurs, with the radius evolving as $r \propto t^m$ where m is in the range 0.6 to 1 (e.g. Chevalier 1982b), a model often called the ‘‘mini-shell’’ model.

Fitting such a function to our radius measurements, we

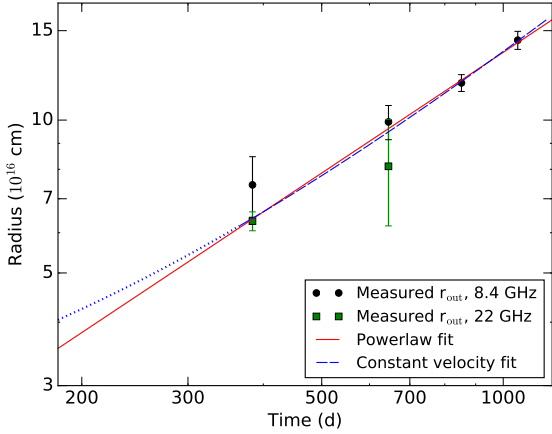


Figure 3. The expansion of SN 2014C. The outer radii were determined by fitting a spherical shell model directly to the visibilities (see Table 2), and calculated for a distance of $D = 15.1$ Mpc. The squares (green) show the values at 22 GHz, and the circles (black) show the values at 8.4 GHz. The age is calculated assuming an explosion date of 2013 December 30. We show two different functions fitted to the measured radii. The first, shown by the solid (red) line, is an uninterrupted powerlaw expansion of the form $r \propto t^m$. The second, shown by the dashed (blue) line, is a constant velocity expansion after $t = 1$ yr (with an implied more rapid expansion before then). We expect the approximately constant-velocity regime to begin at $t \sim 1$ yr, hence we show the extrapolation of the constant velocity fit to earlier times with a dotted line. Note that in this logarithmic plot, the powerlaw expansion produces a straight line, while the constant velocity produces a curved line.

obtain:

$$r_{16} = (6.16 \pm 0.19) \cdot \left(\frac{t}{1 \text{ yr}} \right)^{(0.79 \pm 0.04)} \left(\frac{D}{15.1 \text{ Mpc}} \right).$$

with of $\chi_4^2 = 2.19$, for four degrees of freedom. This corresponds to a velocity of

$$v = (15355 \pm 910) \cdot \left(\frac{t}{1 \text{ yr}} \right)^{(-0.21 \pm 0.04)} \left(\frac{D}{15.1 \text{ Mpc}} \right) \text{ km s}^{-1}.$$

We plot the fitted expansion curve as the red line Figure 3.

The fitted expansion curve, with $m = 0.79$, suggests a moderate amount of deceleration. This value is consistent with what is generally expected from the mini-shell model. If the CSM has a wind density profile ($\rho \propto r^{-2}$), then the mini-shell solution has that $m = (n - 3)/(n + 2)$ (Chevalier 1982b), so this value of m suggests ejecta with $\rho \propto r^{-n}$ with $n = 6.9_{-1.3}^{+0.8}$.

However, SN 2014C is quite an unusual SN, and as already mentioned, there strong evidence that the expanding shock encountered a region of dense H-rich CSM at around $t \sim 130$ d. The expected evolution in this case differs from the self-similar powerlaw function characterizing the evolution of the mini-shell model. Similar systems have been considered by, e.g., Chevalier & Liang (1989); Chugai & Chevalier (2006); Smith & McCray (2007); van Marle et al. (2010). At the point where the shock first encounters the dense shell, it slows dramatically. As the shock progresses through the dense shell, it accelerates again due to the push from the

ever-denser undecelerated ejecta passing through the reverse shock. Once the whole of the massive CSM region has been shocked and accelerated, the expansion continues at almost constant speed until the mass of the CSM swept up from outside the massive shell becomes comparable to the shell mass. This behaviour has been reproduced in numerical simulations by van Marle et al. (2010).

Since the shell impact for SN 2014C occurs before the time of the first VLBI observations at $t = 384$ d, we can not resolve the period of the first interaction with the CSM shell and the slowing of the shock, so we model only the constant velocity expansion after the impact of the shock on the massive shell. Therefore, the second function that we fit to SN 2014C’s expansion, which we call the “constant velocity” function, is $r[t > t_{\text{impact}}] = r_{\text{impact}} + v_{\text{post}} \cdot (t - t_{\text{impact}})$, where t_{impact} is the time at which the shock impacts on the dense shell, r_{impact} is the radius at that time, and v_{post} is the shock velocity after that time. For $t_{\text{impact}} \leq 1$ yr, that function is equal to $r = r_{1\text{yr}} + v_{\text{post}} \cdot (t - 1 \text{ yr})$, so we fit the latter function and avoid the problem of t_{impact} being not exactly known. We again fit the function to the VLBI radius measurements using weighted least squares.³ We obtained

$$r_{16} = (6.19 \pm 0.19) + (4.29 \pm 0.19) \times \left(\frac{t}{1 \text{ yr}} - 1 \right) \left(\frac{D}{15.1 \text{ Mpc}} \right).$$

where the fitted radius at 1 year is $(6.19 \pm 0.19) \times 10^{16}$ cm and post-impact velocity is $v_{\text{post}} = (4.29 \pm 0.19) \times 10^{16}$ cm yr⁻¹, which is equal to 13600 ± 650 km s⁻¹. The χ_4^2 of this fit was 2.02, and we plot the fitted function as the blue line in Figure 3.

The χ_4^2 values for the powerlaw and the constant velocity fitted functions were 2.19 and 2.02 respectively, and therefore our data do not distinguish between these two functional forms, with the constant velocity one providing an only insignificantly better fit. The values of χ^2 are close to the most probable values for four degrees of freedom, indicating a reasonable fit.

5 DISCUSSION

5.1 Morphology of SN 2014C

The VLBI image of SN 2014C at $t = 1057$ d, when we had the highest relative resolution, shows what appears to be a moderately circular source, with a significant brightness enhancement or hot-spot to the W side. Except for this hot-spot, the image is approximately consistent with the morphology expected from a spherically-expanding supernova, which is that of a spherical shell in projection. Such hotspots are seen in the VLBI images of other SNe as well, for example in SN 1986J (Bietenholz & Bartel 2017), SN 1993J (Bietenholz et al. 2003) and SN 2011dh (de Witt et al. 2016). The cause of these asymmetries in the radio brightness is not

³ Note that the powerlaw function above also produces constant-velocity expansion when $m = 1$, but the constant velocity function differs from a power-law one with $m = 1$ in that the intercept is fitted, in other words the extrapolated expansion curve of the constant velocity function is not forced to go through $r = 0$ at $t = 0$.

well known, but they are generally ascribed to asymmetries in the density of the CSM or the ejecta.

5.2 Radius and Expansion Speed

The VLBI measurements show that the radio emission region, the outer edge of which is probably closely associated with the forward shock (see Bartel et al. 2007, for a discussion of this issue in the case of SN 1993J), had a measured radius of $r_{16} = 6.40 \pm 0.26$ at $t = 384$ d, implying an average expansion velocity up to that time of 19300 ± 790 km s⁻¹.

By fitting the 16-GHz lightcurve, Anderson et al. (2017) derive $r_{16} \simeq 0.3$ at $t \simeq 80$ d, implying a velocity of ~ 5000 km s⁻¹. Considerably higher velocities are suggested by spectroscopy, with Milisavljevic et al. (2015) finding velocities of 13000 km s⁻¹ (from Fe II, He I and Ca II absorption lines) at $t = 10$ d, which suggesting that the forward shock must be moving at very least at 13000 km s⁻¹. In fact Milisavljevic et al. (2015) found evidence of a high-velocity H α absorption feature at velocities as high as 21000 km s⁻¹ at $t = 10$ d. Since the fastest H is difficult to detect in absorption, the actual shock velocity is expected to be somewhat higher than 21000 km s⁻¹. In the best-studied case of SN 1993J, the forward shock velocity was $\sim 10\%$ higher than the blue edge of the H α absorption (Bartel et al. 2007), so we can estimate the shock velocity at $t = 10$ d as being $\gtrsim 23000$ km s⁻¹ from the H α absorption.

Our VLBI measurements of an average shock velocity of 19300 ± 790 km s⁻¹ are in agreement with those estimated from optical spectroscopy, but are incompatible with estimates of ~ 5000 km s⁻¹ from Anderson et al. (2017). The estimates of size, and corresponding velocity, at $t \sim 80$ d derived by Anderson et al. (2017) are therefore clearly too small. They were based on the assumption of SSA being the dominant absorption mechanism for the first peak in the 16-GHz lightcurve. Anderson et al. did note the small velocities and questioned whether SSA was in fact the dominant absorption mechanism. They further suggested that the second peak in the 16 GHz lightcurve is due to free-free absorption by the dense CSM. If that were the case, and if the free-free absorbing material were spherically distributed, then there must be significant free-free absorption even for the first lightcurve peak, since the overlying dense CSM had at that point not yet been shocked and was therefore still opaque. Any sizes derived by assuming predominately SSA, such as those of Anderson et al., will be therefore be underestimated.

We can conclude that the shock front was likely expanding at $\gtrsim 23000$ km s⁻¹ at $t = 10$ d. Our powerlaw-function expansion fit to the VLBI measurements after $t = 384$ d, i.e. $r_{16} = (6.16 \pm 0.19) (t/1\text{yr})^{(0.79 \pm 0.04)}$, implies a forward shock velocity at $t = 10$ d of 33000 ± 3200 km s⁻¹, consistent with the lower limit estimated from the H α absorption.

As already mentioned, however, given the strong indications from optical, mid-infrared, X-ray, and radio that SN 2014C's shock encountered dense, H-rich material sometime between a few weeks and the first year after the explosion, an uninterrupted powerlaw expansion seems unlikely. The onset of the strong CSM interaction must have happened sometime before $t = 130$ d, when strong H α lines were first observed (Milisavljevic et al. 2015).

As we discussed in § 4.2, in this case an approximately

constant velocity expansion is expected after the shock has progressed through the region of dense CSM. Since our VLBI radius measurements occur after the impact of the shock on the dense CSM, we fitted (in addition to the powerlaw function), a constant-velocity function to our VLBI radius measurements to accommodate this scenario. The fit of the two functional forms of the expansion is statistically indistinguishable. In other words, unfortunately, our VLBI measurements do not shed much light on the evolution during the critical period between $t = 30$ d and ~ 1 yr when the shock first encountered the dense H-rich material.

Regardless of whether we use the powerlaw or the constant-velocity function for the expansion, however, there must have been a rapid expansion up to the time of the first VLBI measurement at $t = 384$ d, with the average expansion velocity to that time being 19300 ± 790 km s⁻¹. Since the velocity after $t = 384$ d is $\sim 30\%$ lower at $\sim 13600 \pm 650$ km s⁻¹, SN 2014C has been substantially decelerated since the explosion. If we extrapolate the radius from the constant-velocity function backwards in time, and match it to one computed from the 23000 km s⁻¹ early velocity derived from the H α absorption at $t = 10$ d, we can calculate that the break in the expansion curve would have occurred at $t \sim 230$ d. This is somewhat later than $t = 130$ d, when prominent H α emission was already seen in the spectrum, suggesting perhaps an even higher early velocity for the forward shock, or a period of low velocity immediately after the impact, but before our VLBI measurements, such as is seen in the simulations of van Marle et al. (2010), see Figure 4 below.

Our size measurement of $r_{16} = 6.40 \pm 0.26$ at $t = 384$ d gives an upper limit on the outer radius of the dense CSM shell, since our subsequent VLBI measurements show an approximately constant velocity expansion, implying that the shock has already exited the dense CSM shell.

A lower limit on the inner radius of the CSM shell can be obtained by extrapolating our constant velocity fit back to the time of impact, t_{impact} . Lower values of t_{impact} lead to smaller values of the inner radius of the shell. If we take a low value of $t_{\text{impact}} = 30$ d, we obtain $r_{16, \text{extrapolated}} (t = 30 \text{ d})$ of 2.3 ± 0.3 . These values of t_{impact} and r_{16} imply an improbably large pre-impact average speed of 87000 ± 9900 km s⁻¹. We therefore consider somewhat later values of t_{impact} more likely, for example, $t_{\text{impact}} = 80$ d, which implies $r_{16, \text{extrapolated}} (t = 80 \text{ d})$ of 2.8 ± 0.2 and a pre-impact speed of 41000 ± 3500 km s⁻¹. We can therefore constrain the dense CSM shell to be somewhere in the range of $2.8 \lesssim r_{16} \lesssim 6.4$. This range of radii for the dense CSM shell is consistent with the estimates given by Milisavljevic et al. (2015) and Margutti et al. (2017).

These values are only approximate, since the exact evolution of the shock radius around the time of the impact will be much more complicated than an instantaneous transition from one constant velocity to a lower one.

5.3 Comparison to Numerical Models

Van Marle et al. (2010) performed simulations of a Type IIIn SN shock hitting a dense circumstellar shell that show in more detail the dynamics in this case. We compare our measurements of radius as a function of time to the evolution in those simulations. Our comparison is only intended to be illustrative, and we scale the simulated velocity curves of

van Marle et al. 2010 to the case of SN 2014C in a very simple way which incorporates no physics. Specifically, we first scale the times of the simulations so that the impact of the shock on the dense CSM shell occurs at $t = 80$ d, and then subsequently scale the simulation’s velocities so that they match the last one derived from our VLBI observations of SN 2014C, which was 14300 km s^{-1} at $t = 955$ d (§4).

The models of van Marle et al. (2010) covered a wide range of parameter space including CSM shell masses between 0.1 and $25 M_{\odot}$, supernova explosion energies between 0.5×10^{51} and 2×10^{51} erg, stellar wind velocities of 50 to 500 km s^{-1} , and mass-loss rates between 10^{-5} and $10^{-3} M_{\odot} \text{ yr}^{-1}/10 \text{ km s}^{-1}$. The progenitor of SN 2014C was likely a Wolf-Rayet star just before it exploded, with wind velocity values towards the upper end, and mass-loss rates towards the lower end, of those ranges. Van Marle et al.’s models were intended for a situation closer to that of η Carinae, and therefore had dense CSM shells with inner radii of $(0.5 \sim 4) \times 10^{15} \text{ cm}$ which were rather closer to the star at the time of the SN than the one in SN 2014C, which is at $r \sim 6 \times 10^{16} \text{ cm}$. (For further details of the simulations, please see van Marle et al. 2010).

We plot the scaled, simulated velocity curves against our measurements in Figure 4. Because of our simple scaling of the model curves, the true evolution of SN 2014C is not expected to follow the plotted curves in detail. However, we believe that Figure 4 is nonetheless useful to illustrate the general nature of the behaviour. It can be seen that in all the modelled cases (when scaled to match SN 2014C), the initial velocities are quite high, being in the range of $30000 \sim 80000 \text{ km s}^{-1}$, and the velocities then decrease very rapidly by factors of $4 \sim 8$ when the shock impacts on the dense CSM shell, and then recover over the next ~ 200 days and remain relatively constant subsequently. Thus we expect in the case of SN 2014C that there would be very high shock velocities in the first ~ 80 d, before the shock impacted on the dense CSM region, consistent with the $v \geq 21000 \text{ km s}^{-1}$ seen in H α by Milisavljevic et al. (2015). Indeed, shock speeds of ~ 20000 to $\sim 100,000 \text{ km s}^{-1}$ are seen in other Type Ib SNe (Chevalier 2007), so a high (initial) shock speed is consistent with what is expected.

5.4 Radio Absorption and Ionization in the Dense CSM Shell

The dense H-rich CSM must be at least partly transparent to radio waves, otherwise the early radio emission, first detected at $t = 12$ d after shock breakout (Kamble et al. 2014) and at $t = 17$ d at 15 GHz (Anderson et al. 2017) would have been absorbed. If the dense CSM were distributed in a uniform spherical shell, with mass $\sim 1 M_{\odot}$ (Margutti et al. 2017), then the densities must be quite high, and strong free-free absorption would be expected of the shell were ionized. If we take the radius $5.5 \times 10^{16} \text{ cm}$ and thickness 10^{16} cm proposed by Margutti et al. (2017), and assume a uniform density and complete ionization, we can calculate a number density of electrons of $n_e \sim 4 \times 10^6 \text{ cm}^{-3}$, which would have an optical depth at 7 GHz of $\tau_{7\text{GHz}} > 100$. Our VLBI measurements constrain the shell to be somewhere between the radii of $2.8 \times 10^{16} \text{ cm}$ to $6.4 \times 10^{16} \text{ cm}$ (§ 5.2) at the time of impact. Even if we take $1M_{\odot}$ of ionized material uniformly spread out over this whole range, we obtain $n_e \sim 10^6 \text{ cm}^{-3}$

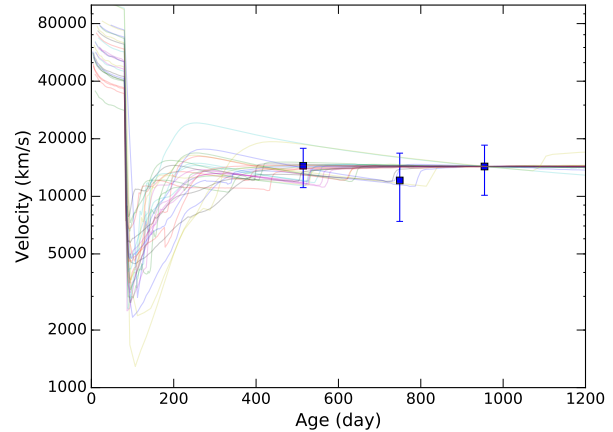


Figure 4. The expansion velocity SN 2014C, compared to scaled simulations of a Type II_n supernova shock hitting a circumstellar shell from van Marle et al. (2010). The three points show the velocities derived from pairs of our VLBI measurements of the outer radius of SN 2014C at four different times along with their uncertainties (see text, § 4). The thin, coloured lines show all the simulations (“A00”, “A01”, . . . “G01”; for a range of different parameters for the explosion and the shell) from van Marle et al. 2010, scaled in time so that the impact occurs at $t = 80$ d, and then scaled in velocity to match the measured value at $t = 954$ d, which was $14300 \pm 4200 \text{ km s}^{-1}$. The figure is intended to be illustrative only since the scaling of the simulated velocity curves does not include any physics.

and $\tau_{7\text{GHz}} \sim 90$. Milisavljevic et al. (2015) and Margutti et al. (2017) derive electron densities of a similar magnitude from the optical spectra and X-ray emission respectively. If the dense CSM shell were uniform and substantially ionized, therefore, no radio emission should have been seen till the shock has progressed through it and heated it to the point where it becomes transparent to radio.

However, as discussed by van Marle et al. (2010), the densities in the shell are likely high enough that substantial recombination would occur, so it is possible that the dense CSM shell was mostly neutral at the time of the SN explosion. Nonetheless, the shock breakout will almost certainly have at least partly ionized the dense CSM shell, therefore a significant amount of free-free absorption of the radio emission is likely to occur in the first year. The exact amount of free-free absorption will depend on the fraction of the CSM shell that is ionized, and would be hard to calculate without detailed modelling.

The other possibility is that the dense CSM was not spherically distributed (note that Anderson et al. 2017, have already suggested this possibility for SN 2014C). The CSM might be non-spherically distributed on small scales, in other words fragmented. Such fragmentation of the CSM is often invoked in the case of Type II SNe (e.g. Weiler et al. 2002) to explain the relatively slow rise of the lightcurves, so some fragmentation of SN 2014C’s dense CSM shell is not unexpected. Alternatively, the dense CSM might be distributed with some large-scale non-spherical geometry, perhaps in the form of an equatorial disk. Such a geometry is also not unexpected, since the CSM structure in SN 1987A is seen to be quite complex (see, e.g. McCray & Fransson 2016). In

the particular case of SN 2014C, Milisavljevic et al. (2015) discuss reasons why the mass loss experienced by the progenitor system may have been strongly asymmetric and how it was potentially driven by interaction between the progenitor star and a close binary companion.

We can conclude that a dense CSM shell must be either largely neutral or rather fragmented for the radio emission from the expanding shock, detected already at $t = 12$ d, to escape before the shock has progressed through the dense CSM shell.

6 SUMMARY AND CONCLUSIONS

We obtained VLBI observations of the unusual supernova SN 2014C, which allowed us to resolve the radio emission from the expanding shell of ejecta, and directly measure the size at several epochs between $t = 384$ and 1057 d after the explosion. We found that:

1. At $t = 384$ d, the angular radius of the supernova was 0.283 ± 0.012 mas, corresponding to $(6.40 \pm 0.26) \times 10^{16}$ cm (for a distance of 15.1 Mpc).
2. This radius corresponds to an average expansion speed up to $t = 384$ d of 19300 ± 790 km s⁻¹.
3. Our VLBI measurements at $t \geq 384$ d show that the average speed between $t = 384$ d and 1057 d was 13600 ± 640 km s⁻¹. Our measurements are compatible with a constant velocity expansion during that period, but a modestly decelerating expansion over that period can not be excluded either.
4. The supernova has clearly been substantially decelerated already *before* our first VLBI measurement, that is, by $t = 384$ d.
5. Our observations are consistent with the scenario, which has already been suggested based on observations at other wavelengths, that SN 2014C's expanding SN forward shock encountered a dense, H-rich CSM shell at $30 \lesssim t \lesssim 130$ d after the explosion. An almost constant velocity expansion is expected after the shock emerges from the dense shell in this case, which is what we have seen in the VLBI measurements.
6. The detection of early radio emission before 30 d implies that the dense H-rich CSM must be largely transparent to radio. This could occur either if the dense CSM was mostly neutral or if it was non-spherically distributed, so that our lines of sight to near the explosion centre bypass most of the dense CSM.

ACKNOWLEDGEMENTS

We thank Allard Jan van Marle for making his simulation data available to us. We thank the anonymous referee for helpful comments. We have made use of NASA's Astrophysics Data System Abstract Service. This research was supported by both the National Sciences and Engineering Research Council of Canada and the National Research Foundation of South Africa.

REFERENCES

Anderson G. E., et al., 2017, MNRAS, 466, 3648

- Bartel N., Bietenholz M. F., 2016, in Supernova Remnants: An Odyssey in Space after Stellar Death. p. 133
- Bartel N., et al., 2002, ApJ, 581, 404
- Bartel N., Bietenholz M. F., Rupen M. P., Dwarkadas V. V., 2007, ApJ, 668, 924
- Bietenholz M., 2014a, in Tarchi A., Giroletti M., Feretti L., eds, 12th European VLBI Network Symposium and Users Meeting (2014), published by SISSA, Trieste. p. 51
- Bietenholz M. F., 2014b, PASA, 31, 2
- Bietenholz M. F., Bartel N., 2017, ApJ, 839, 10
- Bietenholz M. F., Bartel N., Rupen M. P., 2003, ApJ, 597, 374
- Bietenholz M., et al., 2010, in 10th European VLBI Network Symposium and EVN Users Meeting: VLBI and the New Generation of Radio Arrays. , arXiv:1103.1783
- Chevalier R. A., 1982a, ApJ, 258, 790
- Chevalier R. A., 1982b, ApJ, 259, 302
- Chevalier R. A., 2007, in Revista Mexicana de Astronomia y Astrofisica Conference Series. pp 41–48
- Chevalier R. A., Irwin C. M., 2011, ApJL, 729, L6
- Chevalier R. A., Liang E. P., 1989, ApJ, 344, 332
- Chugai N. N., Chevalier R. A., 2006, ApJ, 641, 1051
- Dwarkadas V. V., 2005, ApJ, 630, 892
- Jun B., Norman M. L., 1996, ApJ, 465, 800
- Kamble A., Soderberg A., Zauderer B. A., Chakraborti S., Margutti R., Milisavljevic D., 2014, The Astronomer's Telegram, 5763
- Kim M., et al., 2014, Central Bureau Electronic Telegrams, 3777
- Kudritzki R.-P., Puls J., 2000, Ann. Rev. Astron. Astrophys., 38, 613
- Marcaide J. M., et al., 1997, ApJL, 486, L31
- Margutti R., et al., 2017, ApJ, 835, 140
- McCray R., Fransson C., 2016, Ann. Rev. Astron. Astrophys., 54, 19
- McIntosh A., 2016, ArXiv e-prints
- Milisavljevic D., et al., 2013, ApJ, 767, 71
- Milisavljevic D., et al., 2015, ApJ, 815, 120
- Nugis T., Lamers H. J. G. L. M., 2000, Astron. Astrophys., 360, 227
- Saha A., Thim F., Tammann G. A., Reindl B., Sandage A., 2006, ApJS, 165, 108
- Smith N., 2014, Ann. Rev. Astron. Astrophys., 52, 487
- Smith N., McCray R., 2007, ApJL, 671, L17
- Soderberg A. M., Chevalier R. A., Kulkarni S. R., Frail D. A., 2006, ApJ, 651, 1005
- Tartaglia L., Pastorello A., Benetti S., Cappellaro E., Tomasella L., Ochner P., Elias-Rosa N., Turatto M., 2014, The Astronomer's Telegram, 5742
- Tinyanont S., et al., 2016, ApJ, 833, 231
- Vinko J., et al., 2017, ApJ, 837, 62
- Weaver R., McCray R., Castor J., Shapiro P., Moore R., 1977, ApJ, 218, 377
- Weiler K. W., Panagia N., Montes M. J., Sramek R. A., 2002, Ann. Rev. Astron. Astrophys., 40, 387
- Wellons S., Soderberg A. M., Chevalier R. A., 2012, ApJ, 752, 17
- Zauderer B. A., Kamble A., Chakraborti S., Soderberg A., 2014, The Astronomer's Telegram, 5764
- de Witt A., Bietenholz M. F., Kamble A., Soderberg A. M., Brunthaler A., Zauderer B., Bartel N., Rupen M. P., 2016, MNRAS, 455, 511

van Marle A. J., Smith N., Owocki S. P., van Veelen B.,
2010, MNRAS, 407, 2305